

Control of Extraordinary Optical Transmission in Resonant Terahertz Gratings via Lateral Depletion in an AlGaN/GaN Heterostructure

Geofrey Nyabere¹, Hunter Ellis¹, Miguel Gomez¹, Wei Jia¹, Yizheng Liu², Karli Ann Higley¹, Sriram Krishnamoorthy², Steve Blair¹, Kai Fu¹, and Berardi Sensale-Rodriguez^{1,*}

¹ Department of Electrical and Computer Engineering, The University of Utah, Salt Lake City, UT 84112, USA

² Materials Department, University of California Santa Barbara, Santa Barbara, CA 93106, USA

* Corresponding author, e-mail: berardi.sensale@utah.edu

Abstract

Periodic metallic gratings on substrates can support a range of electromagnetic modes, such as leaky waveguide, guided-resonant, and Fabry-Pérot (FP) cavity modes, which can strongly modulate optical transmission under resonant excitation. Here, we investigate how this coupling can be dynamically manipulated through charge-density control in a laterally patterned AlGaN/GaN heterostructure. The structure comprises metallic stripes separated by regions containing a two-dimensional electron gas (2DEG), forming a periodically modulated interface whose electromagnetic response is governed by the charge density between the stripes. In the unbiased state, the conductive 2DEG screens the incident terahertz field and suppresses excitation of guided modes. When the 2DEG is depleted, the change in boundary conditions allows efficient coupling into substrate resonances, producing a strong modulation at particular frequencies where extraordinary optical transmission (EOT) through the structure takes place. The results highlight the sensitive dependence of guided-mode-resonance (GMR) mediated EOT on inter-stripe charge distribution and demonstrate a direct interplay between carrier dynamics and resonant electromagnetic phenomena in the terahertz regime.

I. INTRODUCTION

Active control of the electromagnetic wave propagation in the terahertz (THz) frequency range is of critical importance for applications in imaging, spectroscopy, and next-generation wireless communications. In this context, the earliest electrically driven THz modulators were reported by Kleine-Ostmann *et al* in the mid-2000s, who employed carrier depletion in a two-dimensional electron gas (2DEG) heterostructure to achieve room-temperature modulation of THz transmission¹. Subsequent work by the same group investigated the spatial distribution of the depletion region and its effect on modulation efficiency, establishing the basic principles of semiconductor-based THz modulators². Although these early devices demonstrated proof-of-concept electrical tunability, their performance was limited by the modest modulation depth and speed attainable through direct control of carrier density in large-area structures.

A significant advance was achieved with the advent of metamaterial-based modulators. Herein, Chen *et al* demonstrated the first active THz metamaterial device by integrating semiconductor layers with resonant metallic elements, enabling strong modulation of transmitted amplitude through electrical excitation³. Work by Shrekenhamer *et al.* subsequently incorporated high-electron-mobility transistors into metamaterial unit cells, realizing high-speed modulation with enhanced interaction between the electromagnetic resonance and the active medium⁴. These works established metamaterial approaches as an effective route to increase modulation depth by concentrating the electric field in subwavelength resonators.

The introduction of novel tunable materials further expanded the design space for active THz devices. Graphene, with its gate-tunable carrier density and high mobility, enabled modulators with near-unity amplitude modulation and low insertion loss^{5,6}. Similarly, vanadium dioxide (VO₂) was used to realize thermal or optically driven modulators that exploit the insulator-to-metal phase transition to achieve large contrast ratios^{7,8}. These developments demonstrated the potential of combining resonant structures with materials enabling dynamic conductivity control.

In parallel, periodic metallic gratings and all-dielectric metasurfaces have emerged as versatile platforms for manipulating THz transmission through guided-mode resonances (GMR) and extraordinary optical transmission (EOT). In this context, Ferraro *et al.* demonstrated narrowband THz filters based on the excitation of guided-mode resonances in thin cyclo-olefin polymer films patterned with metallic stripes or patches, achieving high-Q, high-transmission responses suitable for THz communications applications⁹. Building on this, Bark *et al.* explored all-dielectric GMR filters in the THz region and identified multiple TE and TM resonances with high Q-factors and polarization selectivity, establishing dielectric GMR filters as low-loss, tunable alternatives to metal-based metasurfaces¹⁰. Later work by Bark and Jeon employed the TE-mode GMR of dielectric films to realize sensitive dielectric-film sensors in the THz band¹¹. Jia *et al.* extended these studies to analyze metallic gratings on anisotropic dielectric substrates, revealing the role of

substrate anisotropy on the resonance characteristics and demonstrating their application for anisotropic refractive-index characterization¹².

The potential for dynamic control in GMR systems has been further demonstrated through tunable and reconfigurable designs. Miao *et al.* reported a dynamically tunable THz GMR filter fabricated on an elastic styrene–butadiene–styrene (SBS) film, achieving broadband spectral tunability through mechanical strain while preserving narrow linewidth and structural stability¹³. Furthermore, Yao *et al.* demonstrated the versatility of resonant waveguide gratings in optical sensing by integrating FP cavities with guided-mode structures, achieving enhanced resonance strength and compact footprint for refractive-index detection applications¹⁴. From a theoretical analysis, Isic *et al.* also showed that metal–semiconductor–metal metasurface modulators can provide substantial electrical control of resonant reflection in the THz regime¹⁵. Overall, these results establish that GMR and EOT-based architectures, whether metallic or all-dielectric, can simultaneously enable high spectral selectivity, strong field confinement, and tunable functionality, thereby bridging fundamental resonance phenomena with practical THz device applications.

Building upon these advances, the present work explores the control of extraordinary optical transmission in resonant THz gratings through lateral depletion in an AlGaN/GaN heterostructure. By modulating the inter-stripe carrier distribution in a two-dimensional electron gas, the boundary conditions governing guided-mode resonance coupling are dynamically altered, enabling efficient electronic tuning of resonant THz transmission.

II. DEVICE STRUCTURE AND SIMULATIONS

The proposed device consists of an interdigitated metallic grating on a sapphire substrate, as depicted in **Fig. 1(a)**. The geometry is defined by the finger width (w), gap (g), period ($p = w + g$), metal thickness (t), and substrate thickness (h). We performed a two-dimensional full-wave electromagnetic simulation using COMSOL Multiphysics (with results verified in Ansys Electronic Desktop HFSS). The grating parameters were set as follows: $w = 200 \mu\text{m}$, separation gap $g = 3 \mu\text{m}$, metal thickness $t = 300 \mu\text{m}$, and substrate thickness $h = 430 \mu\text{m}$. The structure's periodicity reduced the simulation domain to a single unit cell with periodic boundary conditions defined in the x -direction. A TE-polarized plane wave (electric field oriented perpendicular to the fingers) was normally incident on the structure. The grating was modeled as gold with a finite conductivity of $\sigma_{\text{gold}} = 4.1 \times 10^7 \text{ S/m}$. To illustrate the response of the structure, we analyzed two configurations: (i) a reference grating on a lossless sapphire substrate and (ii) an identical grating with a two-dimensional electron gas (2DEG) layer located just beneath the fingers. The 2DEG was modeled as a conductive sheet impedance, with its frequency-dependent permittivity and conductivity governed by a Drude model¹⁶. Following an approach previously used by our group¹⁷, we fitted an analytical model to measured transmission data through a 2DEG in AlGaN/GaN on sapphire wafer to determine its charge

transport parameters. From this fit, we obtained a mobility of $1,540 \text{ cm}^2/\text{V}\cdot\text{s}$, a sheet density of $1.43 \times 10^{13} \text{ cm}^{-2}$, and a sheet conductivity of 3.50 mS . Contrasting transmission results for (i) and (ii) enables us to predict the dynamic response of the device illustrated in **Fig. 1(b)**.

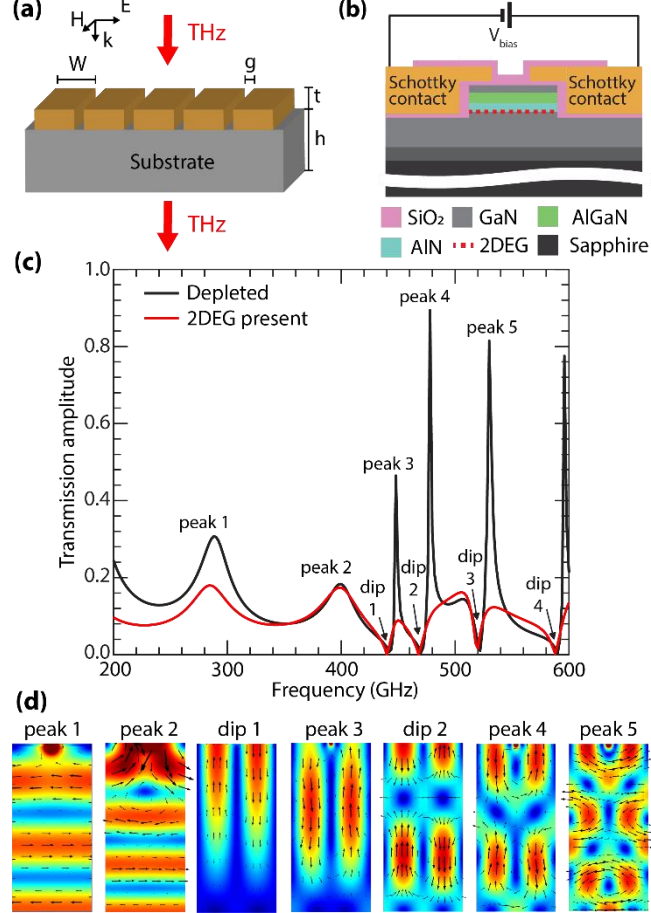


Figure 1. (a) Schematic of the grating structure under normally incident, TE-polarized THz radiation. (b) Biasing scheme for the interdigitated grating, where the applied voltage creates a depletion region to modulate the 2DEG conductivity. (c) The simulated transmission spectrum for a single unit cell shows characteristic FP and GMR. Spectrally narrow EOT peaks at high frequencies vanish when a 2DEG is placed in between the grating metal stripes. (d) Electric field distributions for the resonant peaks and dips labeled in (c), with arrows indicating the local field orientation.

As shown in **Fig. 1(c)**, the simulated transmission spectrum for the reference grating (i) shows two clear resonant regimes. At lower frequencies, the spectrum is characterized by broad Fabry-Pérot (FP) resonances within the substrate, with the N-th order mode approximated by¹²,

$$f_{TEM,N} = \frac{\left(2N - \frac{w}{p}\right)c_0}{4\sqrt{\epsilon_{xx}h}}, \quad (1)$$

where p is the grating period, w is the stripe width, ϵ_{xx} is the in-plane relative substrate permittivity (~9.4 for sapphire), and h is the substrate thickness. For example, the simulated third-order FP mode at 0.288 THz is in excellent agreement with the calculated value of 0.276 THz. At higher frequencies, the response is dominated by sharp guided-mode resonances (GMRs)⁹. These arise when grating-diffracted waves couple into slab waveguide modes supported by the substrate. The general condition for GMRs is given by ¹²,

$$f_{TM,N_x,N_y} = c_0 \sqrt{\left(\frac{N_x}{p\sqrt{\epsilon_{yy}}}\right)^2 + \left(\frac{N_y}{2h\sqrt{\epsilon_{xx}}}\right)^2} \quad (2)$$

where N is the integer mode order, c_0 is the speed of light in vacuum, p is the period, h is the substrate height, ϵ_{xx} is the in-plane, and ϵ_{yy} the out-of-plane (~11.5 for sapphire) substrate relative permittivity. For odd order modes, $\frac{1}{2}$ is added to the N_y value. In our spectrum, even-order modes appear as transmission peaks (e.g., at 448, 478, and 530 GHz) due to constructive interference, while odd-order modes appear as dips (e.g., at 442, 470, 522, and 590 GHz) due to destructive interference.

Analysis of the simulated electric field distributions (**Fig. 1(d)**) confirms this behavior. The transmission peaks (3, 4) correspond to even modes with symmetric field profiles, while the dips (1, 2) correspond to odd modes with antisymmetric profiles. Similar to subwavelength slot antennas, the fields are strongly confined within the gaps and enhanced at the metal edges⁹. This strong localization is crucial for efficient coupling to the substrate modes, dictating transmission features. This observation also holds critical importance for the active operation of the device when controlling charge in the 2DEG.

When the 2DEG layer is included, the transmission spectrum changes noticeably. The grating becomes more reflective, and the sharp guided-mode resonance (GMR) peaks are strongly suppressed, as shown in **Fig. 1(c)**. The effect is more pronounced for the highest-Q resonances. At zero bias, the free carriers in the 2DEG effectively short the capacitive gaps of the grating, preventing the resonant field build-up required for efficient transmission and causing the incident THz wave to be reflected. The broader FP background is less sensitive to field confinement and changes very little. In contrast, the transmission peak at 478 GHz is strongly reduced. This shows the strong influence of the conductive channel. In an actual device, the 2DEG conductivity can be tuned with an applied voltage across the metal stripes (electrodes). The “no-2DEG” condition corresponds to a fully depleted channel, which occurs when a large enough reverse bias is applied between adjacent fingers acting as Schottky contacts (**Fig. 1(b)**). This applied voltage expands

the depletion region laterally. By adjusting the applied voltage, the 2DEG can be partially or fully depleted, allowing control over the resonant THz transmission.

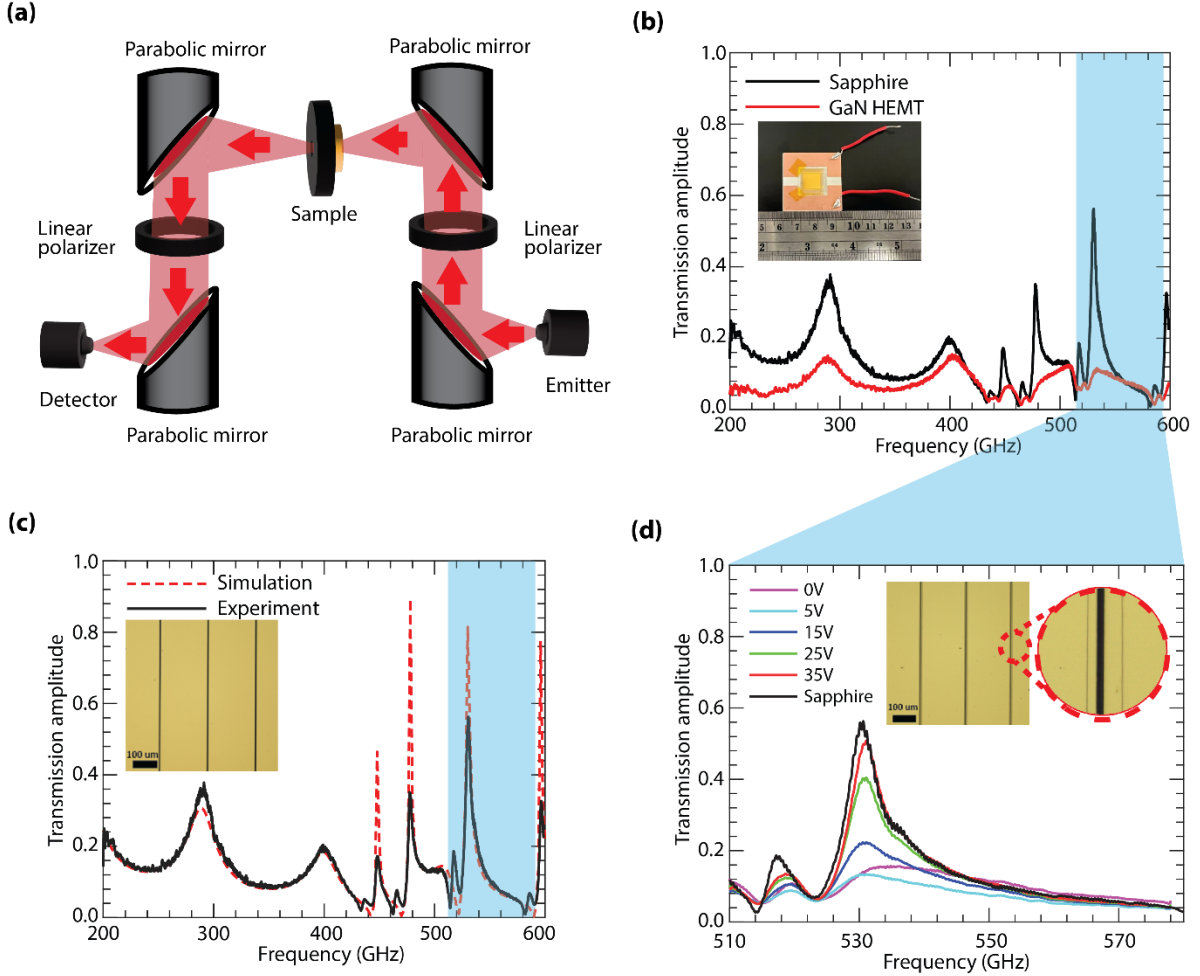


Figure 2. (a) Diagram of the frequency-domain THz spectrometer employed for device characterization. (b) Transmission spectra measured for the reference grating (black) and the AlGaN/GaN active device at zero bias (red). The presence of the 2DEG makes the EOT resonant features vanish from the measured spectra. Inset: microscope image of the active device. (c) Measured (solid) versus simulated (dashed) transmission for the passive reference grating on sapphire, showing close agreement in the position of spectral features. Inset: optical image of the fabricated reference device. (d) Transmission of the active device under reverse bias ranging from 0 V to 35 V. As the 2DEG is depleted, the EOT peak becomes more pronounced. Inset: zoomed-in view of the interdigitated fingers and mesa.

III. EXPERIMENTAL RESULTS AND DISCUSSION

We fabricated two devices: an active grating on an AlGaN/GaN heterostructure and a passive reference grating on a bare sapphire substrate. For the active device, we used a commercial AlGaN/GaN

heterostructure grown on a 430 μ m thick *c*-plane sapphire substrate. The epitaxial structure consists of a 3nm GaN cap, a 21nm AlGaN barrier, a 1nm AlN spacer, and a 1.8 μ m GaN channel. A 2DEG naturally forms at the AlGaN/GaN interface. For the active sample, the first fabrication step was mesa isolation, which was performed using a BCl_3/Cl_2 plasma etch at 100 W to a depth of approximately 100 nm. After removing the resist, we deposited a very thin SiO_2 layer (\sim 3 nm) by atomic layer deposition (ALD) at 200°C. This layer helps raise the breakdown voltage. We patterned a bilayer resist to form the interdigitated Schottky contacts, giving an undercut profile needed for lift-off. A Ni/Au stack (30 nm/270 nm) was then deposited by e-beam evaporation, and the excess was lifted off in acetone. To end, the device was passivated with a thin SiO_2 film (\sim 30 nm) using RF sputtering. For comparison, we also fabricated a reference device with the same grating layout on bare sapphire, but in this case, only photolithography and Ni/Au metallization steps were performed.

The devices' frequency-domain transmission characteristics were measured with a commercial fiber-coupled spectrometer (TOPTICA TeraScan) at room temperature. As shown schematically in **Fig. 2(a)**, a linearly polarized THz beam (TE polarization) was focused onto the device at normal incidence. We performed a broadband (0.2–0.6 THz) transmission measurement of both the passive reference device and the active AlGaN/GaN device at zero bias. Furthermore, the active device was characterized in the 0.51–0.58 THz range by sweeping a DC bias of 0 to 35 V across adjacent fingers, which tunes the depletion of the two-dimensional electron gas and drives the modulation response. The profound effect of the 2DEG depletion is shown in **Fig. 2(b)**, which compares the spectra of the passive and active devices at zero bias. In contrast to the resonant response of the passive device, with strong EOT transmission peaks at frequencies above 0.42 THz, the active device spectrum shows these features suppressed. Normalized transmission levels at these peaks drop from near 0.6 down to about 0.1. The resonance is suppressed because of the conductive 2DEG. At zero bias, the free carriers provide a high conductive path across the grating gaps, effectively turning the structure reflective. This reflective channel screens the resonant fields and prevents the buildup needed to sustain high-Q features¹⁸.

Figure 2(c) shows that our electromagnetic model agrees with the measured spectrum of the passive reference device. The model also captures the positions of the broad FP oscillations and the sharp high-Q guided-mode resonances. The narrow resonances' slightly lower measured peak transmission likely comes from added losses due to fabrication imperfections (lithography and metal losses) as well as misalignments during measurements. High-Q modes are especially sensitive to slight variations in the subwavelength gaps¹².

Figure 2(d) illustrates active modulation. The interdigitated structure acts as an array of back-to-back Schottky diodes¹⁹. When a voltage is applied between adjacent fingers, one junction is driven into forward

bias while the other is reverse-biased. The reverse-biased junction sets the device's electrical response, which limits the current flow. As the reverse bias increases, the 2DEG beneath the biased finger is gradually depleted laterally, narrowing the conductive channel and restoring the grating's resonant response. At 35 V, the transmission peak reaches its maximum value. At 0.53 THz, the modulation depth at resonance is calculated to be about 72%, based on the definition $(T_{max}-T_{min})/T_{max}$. For comparison, the spectrum of the passive reference device is overlaid, representing the maximum achievable transmission if there was no 2DEG. The fact that the modulated peak does not fully reach the reference level suggests that even at 35 V, the 2DEG is not completely depleted across the entire channel, leaving residual free-carrier absorption that limits the ultimate modulation contrast. It is to be mentioned that at modest bias (up to about 10 V), depletion is primarily vertical, occurring directly beneath the Schottky contact. As the voltage is increased, the depletion region begins to extend laterally from the contact edges into the channel, marking the onset of lateral depletion. Such lateral encroachment is significant, as it directly governs the degree of channel pinch-off and therefore the modulation efficiency of the device. It is important to note that the total capacitance of these AlGaN/GaN-based diodes includes components from both the vertical depletion under the contacts and the lateral depletion near the contact edge, along with parasitic capacitance²⁰.

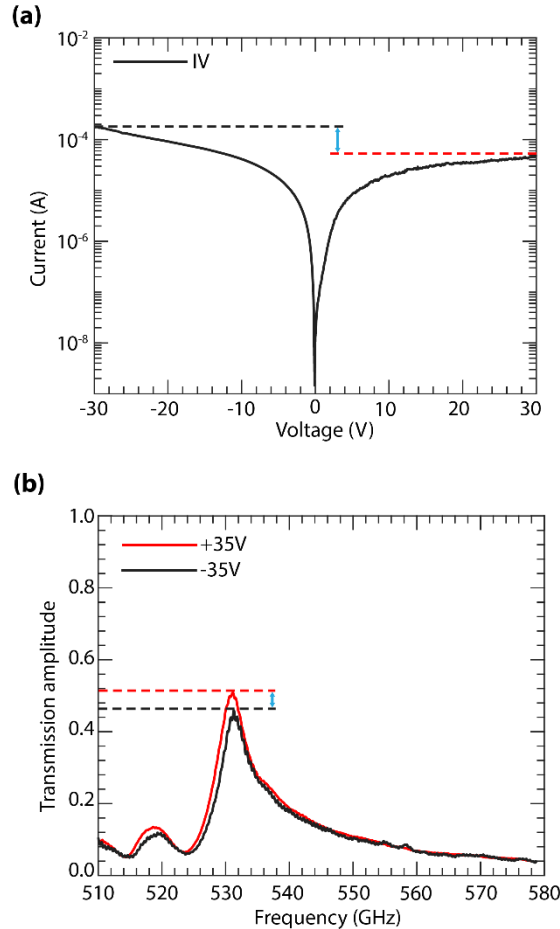


Figure 3. (a) Current-voltage (I-V) characteristic of the device. The distinct asymmetry indicates that the back-to-back Schottky contacts have unequal barrier heights, a result of non-uniformities at the metal-semiconductor interface. (b) Corresponding THz transmission spectrum. The difference in the barrier heights leading to the I-V asymmetry shown in (a) results in the device's bias-asymmetric THz response.

The devices' current-voltage (I-V) characteristics were measured using a Keithley 4200A-SCS Parameter Analyzer. The I-V curve in **Fig. 3(a)** is clearly asymmetric, suggesting that the two back-to-back Schottky contacts have different barrier heights. This effect can still arise even if the contacts are made under identical conditions, because of minor, uncontrollable variations at the metal–semiconductor interface¹⁹. The Schottky barrier height is a key factor for DC leakage and affects the THz modulation. A smaller barrier leads to much higher reverse leakage current and reduces how effectively the 2DEG channel can be depleted. Given this asymmetry, the device's modulation was characterized by sweeping the bias in both polarities to demonstrate the asymmetry of depletion effect on THz transmission clearly. This difference in the electrical barriers is directly reflected in the THz transmission response shown in **Fig. 3(b)** with larger transmission attainable for positive voltages.

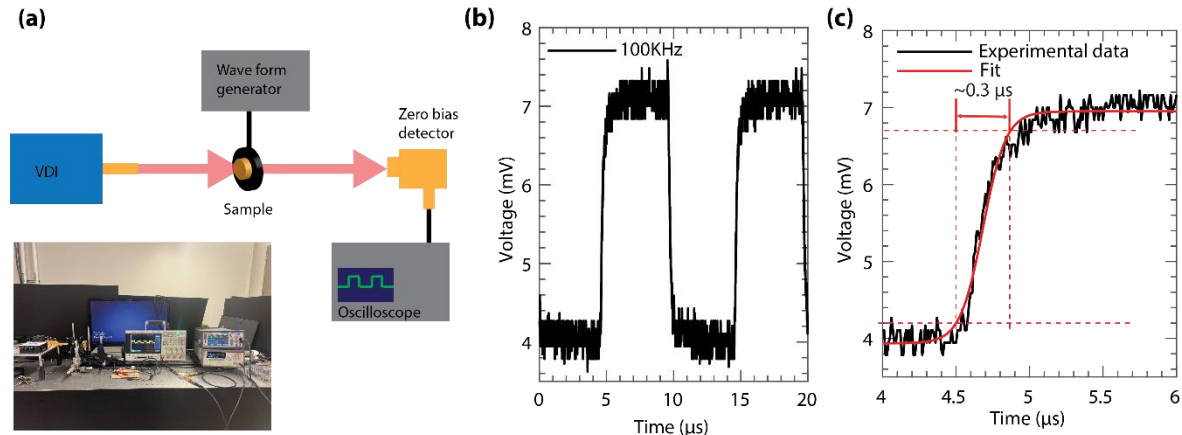


Figure 4. Dynamic characterization. (a) Schematic and optical image of the measurement setup. (b) Modulated THz signal at the detector in response to a 100 kHz square-wave input. (c) Magnified view of the rising edge from (b), indicating a 10–90% rise time of approximately 0.3 μ s.

The device dynamic response was measured using a 0.3 THz continuous-wave (CW) multiplier-based THz source from VDI, a zero-bias detector (ZBD), and an oscilloscope as illustrated in **Fig. 4(a)**. We drove the grating with a square-wave voltage consisting of an AC signal of 10 V (peak-to-peak) riding on a DC bias of 15V that depletes the channel. The modulator's time-response (signal detected by the ZBD) is plotted in **Fig. 4(b-c)**. The oscilloscope trace shows a 10–90% rise time of about 0.3 μ s, corresponding to a cutoff frequency of roughly 1 MHz. The extrinsic RC time constant of the large-area device architecture governs

this measured speed. Note that the modulation depth is about 43%; the drive voltage in this case swings from 10 to 20V and the source frequency is 0.3 THz, which corresponds to a spectral region where the response is dominated by FP resonances; this is different from the modulation attained at the maximum resonance region of 0.53 THz. We estimated the intrinsic cutoff frequency from the device's total series resistance and junction capacitance. When about $\sim 15 \Omega$ resistance from the metal components (such as the bus bar) is considered, the intrinsic speed reaches roughly 220 MHz. The discrepancy between the measured bandwidth and the intrinsic device speed is due to significant resistance and capacitance (RC constant)^{21,22}. These parasitics arise from series resistance in the forward-biased Schottky contact, undepleted 2DEG channel, metallic traces, and parasitic capacitances from the interdigitated fingers and contact pads. Although the performance is below the intrinsic limits of GaN, this first-generation prototype successfully demonstrates that the active free-space modulator is a viable and effective mechanism for THz modulation. Future work will be devoted to increasing the device speed by minimizing parasitics and reducing the active area, making GHz-class operation possible.

IV. CONCLUSIONS

In summary, we have realized an electrically tunable terahertz modulator based on an interdigitated Schottky grating integrated with an AlGaN/GaN heterostructure. The applied bias laterally depletes the two-dimensional electron gas, enabling dynamic control of coupling between the incident field and guided-mode resonances in the substrate. This change in charge distribution governs the strength of the extraordinary optical transmission observed near 0.53 THz. The measured spectra show excellent agreement with full-wave electromagnetic simulations, validating the resonance-based modulation mechanism. The structure achieves a maximum modulation depth of 72% and a switching speed with associated cut-off frequency of approximately 1 MHz, demonstrating that lateral carrier control provides an efficient means to tune resonant field coupling in the terahertz regime.

Acknowledgments

This work was supported by the University of Utah research foundation under seed grant “Advancing High-Speed THz Modulators with Lateral GaN Junctions”. This material is also based upon work supported by the Air Force Office of Scientific Research (AFOSR) under Award No. FA9550-18-1-0332. Any opinions, findings, and conclusions or recommendations expressed in this material are those of the author(s) and do not necessarily reflect the views of the United States Air Force. This work was performed in part at the Utah Nanofab sponsored by the College of Engineering, Office of the Vice President for Research, and the Utah Science Technology and Research (USTAR) initiative of the State of Utah.

Author Declarations:

Conflict of Interest

The authors have no conflicts to disclose.

Author Contributions

Geofrey Nyabere: Conceptualization (equal); Data curation (lead); Formal analysis (lead); Investigation (lead); Methodology (lead); Visualization (equal); Writing–original draft (lead); **Hunter Ellis:** Investigation (supporting); Methodology (supporting). **Miguel Gomez:** Investigation (supporting); Methodology (supporting). **Wei Jia:** Investigation (supporting); Methodology (supporting); Formal analysis (supporting); Writing – review & editing (supporting). **Yizheng Liu:** Investigation (supporting); Methodology (supporting). **Karli Ann Higley:** Data curation (supporting); Investigation (supporting). **Sriram Krishnamoorthy:** Investigation (supporting); Methodology (supporting). **Steve Blair:** Investigation (supporting), Methodology (supporting); Formal analysis (supporting); Writing – review & editing (supporting). **Kai Fu:** Funding acquisition (supporting); Resources (supporting); Formal analysis (supporting); Methodology(supporting); Writing – review & editing (supporting). **Berardi Sensale-Rodriguez:** Conceptualization (equal); Funding acquisition (lead); Supervision (lead); Formal analysis (equal); Project administration (lead); Resources (lead); Writing -original draft (equal); Writing – review & editing (lead).

Data Availability

The data that support the findings of this study are available from the corresponding author upon reasonable request.

References

- ¹ T. Kleine-Ostmann, P. Dawson, K. Pierz, G. Hein, and M. Koch, “Room-temperature operation of an electrically driven terahertz modulator,” *Appl. Phys. Lett.* **84**(18), 3555–3557 (2004).
- ² T. Kleine-Ostmann, K. Pierz, G. Hein, P. Dawson, M. Marso, and M. Koch, “Spatially resolved measurements of depletion properties of large gate two-dimensional electron gas semiconductor terahertz modulators,” *J. Appl. Phys.* **105**(9), 093707 (2009).
- ³ H.-T. Chen, W.J. Padilla, J.M.O. Zide, A.C. Gossard, A.J. Taylor, and R.D. Averitt, “Active terahertz metamaterial devices,” *Nature* **444**(7119), 597–600 (2006).
- ⁴ D. Shrekenhamer, S. Rout, A.C. Strikwerda, C. Bingham, R.D. Averitt, S. Sonkusale, and W.J. Padilla, “High speed terahertz modulation from metamaterials with embedded high electron mobility transistors,” *Opt. Express* **19**(10), 9968 (2011).
- ⁵ R. Xia, N.W. Almond, W. Tadbier, S.J. Kindness, R. Degl’Innocenti, Y. Lu, A. Lowe, B. Ramsay, L.A. Jakob, J. Dann, S. Hofmann, H.E. Beere, S.A. Mikhailov, D.A. Ritchie, and W. Michailow, “Achieving 100% amplitude modulation depth in the terahertz range with graphene-based tuneable capacitance metamaterials,” *Light Sci. Appl.* **14**(1), 256 (2025).

⁶ B. Sensale-Rodriguez, R. Yan, M.M. Kelly, T. Fang, K. Tahy, W.S. Hwang, D. Jena, L. Liu, and H.G. Xing, “Broadband graphene terahertz modulators enabled by intraband transitions,” *Nat. Commun.* **3**(1), 780 (2012).

⁷ H. Ma, Y. Wang, R. Lu, F. Tan, Y. Fu, G. Wang, D. Wang, K. Liu, S. Fan, K. Jiang, and X. Zhang, “A flexible, multifunctional, active terahertz modulator with an ultra-low triggering threshold,” *J. Mater. Chem. C* **8**(30), 10213–10220 (2020).

⁸ X. Chen, X. Lu, L. Tang, K. Chen, and W. Huang, “Freestanding and scalable VO₂ /CMC composite film for thermal and optical THz modulation,” *Opt. Express* **33**(6), 13895 (2025).

⁹ A. Ferraro, D.C. Zografopoulos, R. Caputo, and R. Beccherelli, “Guided-mode resonant narrowband terahertz filtering by periodic metallic stripe and patch arrays on cyclo-olefin substrates,” *Sci. Rep.* **8**(1), 17272 (2018).

¹⁰ H.S. Bark, G.J. Kim, and T.-I. Jeon, “Transmission characteristics of all-dielectric guided-mode resonance filter in the THz region,” *Sci. Rep.* **8**(1), 13570 (2018).

¹¹ H.S. Bark, and T.-I. Jeon, “Dielectric film sensing with TE mode of terahertz guided-mode resonance,” *Opt. Express* **26**(26), 34547 (2018).

¹² W. Jia, M. Lou, P. Gopalan, A. Bhattacharyya, S. Krishnamoorthy, and B. Sensale-Rodriguez, “On the terahertz response of metal-gratings on anisotropic dielectric substrates and its prospective application for anisotropic refractive index characterization,” *J. Appl. Phys.* **131**(19), 193101 (2022).

¹³ Y. Miao, J. Wei, M. Xu, Q. Wang, and X. Jiang, “Dynamic Terahertz Guided-Mode Resonance Filter for Broadband Tunability,” *ACS Appl. Polym. Mater.* **6**(13), 7669–7678 (2024).

¹⁴ Y. Yao, Y. Xie, N.-K. Chen, I. Pfalzgraf, S. Suntsov, D. Kip, and Y. Ren, “Design of Fiber-Tip Refractive Index Sensor Based on Resonant Waveguide Grating with Enhanced Peak Intensity,” *Appl. Sci.* **11**(15), 6737 (2021).

¹⁵ G. Isic, G. Sinatkas, D.C. Zografopoulos, B. Vasic, A. Ferraro, R. Beccherelli, E.E. Kriezis, and M. Belic, “Electrically Tunable Metal–Semiconductor–Metal Terahertz Metasurface Modulators,” *IEEE J. Sel. Top. Quantum Electron.* **25**(3), 1–8 (2019).

¹⁶ H.O. Condori Quispe, A. Chanana, J. Encomendero, M. Zhu, N. Trometer, A. Nahata, D. Jena, H.G. Xing, and B. Sensale-Rodriguez, “Comparison of unit cell coupling for grating-gate and high electron mobility transistor array THz resonant absorbers,” *J. Appl. Phys.* **124**(9), 093101 (2018).

¹⁷ R. Yan, S. Arezoomandan, B. Sensale-Rodriguez, and H.G. Xing, “Exceptional Terahertz Wave Modulation in Graphene Enhanced by Frequency Selective Surfaces,” *ACS Photonics* **3**(3), 315–323 (2016).

¹⁸ M.T. Nouman, H.-W. Kim, J.M. Woo, J.H. Hwang, D. Kim, and J.-H. Jang, “Terahertz Modulator based on Metamaterials integrated with Metal–Semiconductor–Metal Varactors,” *Sci. Rep.* **6**(1), 26452 (2016).

¹⁹ A.J. Chiquito, C.A. Amorim, O.M. Berengue, L.S. Araujo, E.P. Bernardo, and E.R. Leite, “Back-to-back Schottky diodes: the generalization of the diode theory in analysis and extraction of electrical parameters of nanodevices,” *J. Phys. Condens. Matter* **24**(22), 225303 (2012).

²⁰ Q. Li, X. Kang, H. Wu, R. Zhao, Y. Zheng, H. Shang, X. Liu, and C. Huang, “Capacitance reduction in AlGaN/GaN heterojunction diodes through thermally oxidized NiO anode,” *Jpn. J. Appl. Phys.* **63**(9), 094003 (2024).

²¹ X. Zhang, Y. Xing, Q. Zhang, Y. Gu, Y. Su, and C. Ma, “High speed terahertz modulator based on the single channel AlGaN/GaN high electron mobility transistor,” *Solid-State Electron.* **146**, 9–12 (2018).

²² H.-T. Chen, S. Palit, T. Tyler, C.M. Bingham, J.M.O. Zide, J.F. O’Hara, D.R. Smith, A.C. Gossard, R.D. Averitt, W.J. Padilla, N.M. Jokerst, and A.J. Taylor, “Hybrid metamaterials enable fast electrical modulation of freely propagating terahertz waves,” *Appl. Phys. Lett.* **93**(9), 091117 (2008).